

Similarity solutions for unsteady stagnation point flow

D. Kolomenskiy¹† and H. K. Moffatt²

¹ Centre Européen de Recherche et de Formation Avancée en Calcul Scientifique, 42 avenue Gaspard Coriolis, 31057 Toulouse CEDEX 01, France

² Department of Applied Mathematics and Theoretical Physics, University of Cambridge, Wilberforce Road, Cambridge CB3 0WA, UK

(Received 28 July 2011; revised 10 July 2012; accepted 6 August 2012;
first published online 12 September 2012)

A class of similarity solutions for two-dimensional unsteady flow in the neighbourhood of a front or rear stagnation point on a plane boundary is considered, and a wide range of possible behaviour is revealed, depending on whether the flow in the far field is accelerating or decelerating. The solutions, when they exist, are exact solutions of the Navier–Stokes equations, having a boundary-layer character analogous to that of the classical steady front stagnation point flow. The velocity profiles are obtained by numerical integration of a nonlinear ordinary differential equation. For the front-flow situation, the solution is unique for the accelerating case, but bifurcates for modest deceleration, while for sufficient rapid deceleration there exists a one-parameter family of solutions. For the rear-flow situation, a unique solution exists (remarkably!) for sufficiently strong acceleration, and a one-parameter family again exists for sufficient strong deceleration. Analytic results, which are consistent with the numerical results, are obtained in the limits of strong acceleration or deceleration, and for the asymptotic behaviour far from the boundary.

Key words: boundary layer structure, general fluid mechanics, Navier–Stokes equations

1. Introduction

Stagnation point flow, for which the outer-stream velocity varies linearly with the coordinate parallel to the boundary, is well known for admitting a similarity solution for which the Navier–Stokes equation may be reduced to an ordinary differential equation. This type of solution has been most commonly studied in the context of the flow past a bluff body. A basic example is a circular cylinder of radius R in a flow with a uniform far-field velocity U_∞ . Near the stagnation point at the front surface of the cylinder, for a small distance s measured along the boundary, the outer-stream velocity $U(s) = 2U_\infty \sin s/R$, given by the potential flow theory, can be approximated by a linear function $U(s) = As$, where $A = 2U_\infty/R$.

A similar type of situation is encountered in an entirely different context, namely in the flow near the flapping wings of an insect employing the ‘clap–fling–sweep’ manoeuvre. When the Reynolds number of the wing motion is large, thin unsteady boundary layers develop near the wing surfaces. The outer-stream velocity may be calculated from the potential flow model originally proposed by Lighthill (1973) or

† Email address for correspondence: dkolom@gmail.com

from its extensions that account for the flow separation (see e.g. Edwards & Cheng 1982). The wings are modelled as a pair of flat plates. They rotate in opposite directions about a common point O , at which their ends are joined with a virtual ‘hinge’. Let (r, θ) be the polar coordinates with the origin at O , the line $\theta = 0$ coinciding with the axis of symmetry. At time t , the wings are at $\theta = \alpha(t)$ and $\theta = -\alpha(t)$. Near the hinge point O , the real part of Lighthill’s complex potential takes the form (Kolomenskiy *et al.* 2011)

$$\Phi(r, \theta) = -\frac{d\alpha/dt}{2 \sin 2\alpha} r^2 \cos 2\theta, \tag{1.1}$$

for $\theta < \alpha$ and assuming $0 < \alpha(t) < \pi/2$, $d\alpha/dt > 0$. Thus, the outer-stream velocity at the wings’ upper surfaces is $U(r, t) = \partial\Phi/\partial r|_{\theta=\pm\alpha} = -A(t)r$, where $A(t) = (d\alpha/dt) \cot 2\alpha$. The linear dependence on the coordinate r is similar to the flow about a cylinder discussed above, but the strength A depends on time. It is this problem that has motivated the study of unsteady stagnation point flow presented in this paper.

A wide class of unsteady flows admitting similarity solutions has been identified (see e.g. Burde 1995 and Drazin & Riley 2006, and references therein). Here, we revisit those situations in which the unsteadiness is associated solely with time-variation of the irrotational flow outside the boundary layer. In the bluff body context (and equally in the flapping wing context), there are four situations to consider: accelerating/decelerating flow near a front/rear stagnation point. We aim to find conditions for the existence of similarity solutions in each case, and to determine the structure of the corresponding flows. Much emphasis is placed on the analysis of solutions to the ordinary differential equations that describe the self-similar velocity profiles.

We consider the two-dimensional flow of a viscous incompressible fluid occupying the half-space $y > 0$, either towards or away from a plane rigid boundary located at $y = 0$. We assume that the flow far from the boundary is the plane irrotational strain with streamfunction

$$\Psi(x, y, t) = \pm A(t)xy, \tag{1.2}$$

where $A(t) > 0$, and the plus or minus sign is chosen according as the flow is towards or away from the boundary (i.e. ‘front’ or ‘rear’ stagnation point flow respectively). The streamfunction $\psi(x, y, t)$ of the flow then satisfies the vorticity equation

$$\frac{\partial(\nabla^2\psi)}{\partial t} - \frac{\partial(\psi, \nabla^2\psi)}{\partial(x, y)} = \nu\nabla^4\psi, \tag{1.3}$$

where ν is the kinematic viscosity of the fluid, and the boundary conditions

$$\psi = \partial\psi/\partial y = 0 \quad \text{on } y = 0, \quad \psi \sim \Psi \quad \text{as } y \rightarrow \infty. \tag{1.4}$$

We consider similarity solutions of (1.3) of the form

$$\psi(x, y, t) = (\nu A(t))^{1/2} x f(\eta) \quad \text{where } \eta = y(A(t)/\nu)^{1/2}, \tag{1.5}$$

with corresponding velocity components

$$u = \partial\psi/\partial x = A(t)x f'(\eta), \quad v = -\partial\psi/\partial y = -(\nu A(t))^{1/2} f(\eta). \tag{1.6}$$

Substitution in (1.3) gives the equation

$$f'''' - f'f'' + ff''' = (\kappa/2)(3f'' + \eta f'''), \tag{1.7}$$

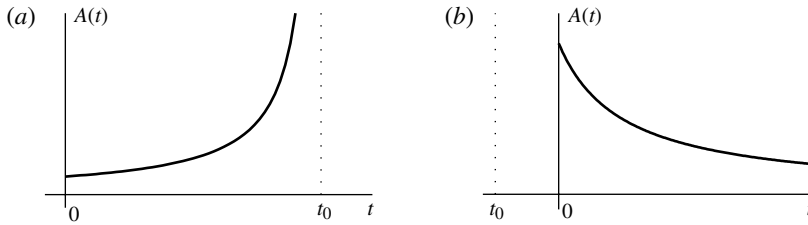


FIGURE 1. Time evolution of the flow strength $A(t)$: (a) accelerating flow, $\kappa > 0$; (b) decelerating flow, $\kappa < 0$. The initial state is at $t = 0$.

where

$$\kappa = \dot{A}/A^2, \quad (1.8)$$

a dimensionless measure of the unsteadiness of the flow (analogous to a Strouhal number). Clearly, (1.7) requires that κ be constant in time, and then (assuming $\kappa \neq 0$), (1.8) integrates to give

$$A(t) = \frac{1}{\kappa(t_0 - t)}, \quad (1.9)$$

where t_0 is constant, such that $A(0) = (\kappa t_0)^{-1} > 0$. Since by assumption $A(t) > 0$, there are two distinct possibilities (as illustrated in figure 1), with initial conditions specified at $t = 0$: accelerating flow with $\kappa > 0$ and $0 \leq t < t_0$, or decelerating flow with $\kappa < 0$ and $t_0 < 0 \leq t < \infty$. In either case, solutions of the form (1.5) have a boundary-layer character, although we note that they are in fact exact solutions of the Navier–Stokes equations. The boundary-layer thickness evidently has order of magnitude

$$\delta \sim (A/\nu)^{-1/2} \sim (\nu\kappa(t_0 - t))^{1/2}, \quad (1.10)$$

approaching a singularity at finite time $t = t_0 > 0$ in the case of accelerating flow, or evolving from a virtual singularity at $t = t_0 < 0$ in the case of decelerating flow. For the case of rear stagnation point flow, we shall find that similarity solutions of the form (1.5) exist only if $|\kappa| \geq 2$; note that for $|\kappa| \gg 2$, the first term on the left-hand side of (1.3) dominates over the second term, i.e. the linear contribution to acceleration dominates over the nonlinear (convective) contribution.

The boundary conditions on $f(\eta)$ are immediately obtained from (1.4) in the form

$$f(0) = f'(0) = 0, \quad f'(\infty) = \pm 1, \quad (1.11)$$

where again the plus or minus corresponds to front or rear stagnation point flow, respectively.

The steady case ($\kappa = 0$) of flow towards a stagnation point was first studied by Hiemenz (1911), and is one of the standard situations considered in boundary-layer theory (Schlichting 1960, § V.8). For flow away from a (rear) stagnation point, by contrast, there is no steady solution of (1.7) satisfying the outer boundary condition $f'(\infty) = -1$; in this situation, a flow reversal takes place in the boundary layer formed during an impulsive start, then the boundary-layer equations break down at a finite time; see the related discussion in the book by Drazin & Riley (2006). When $\kappa \neq 0$, the existence of solutions of (1.7) satisfying the appropriate boundary conditions cannot be taken for granted. Our aim in this note is to explore the range of values

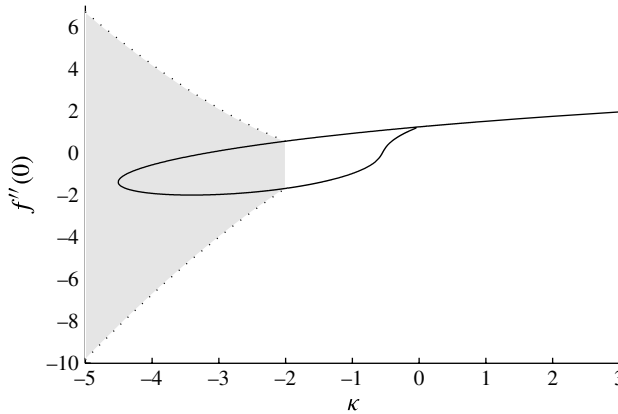


FIGURE 2. Velocity gradient at the wall in flows towards a stagnation point. Any pair of $(\kappa, f''(0))$, lying either on the solid line or in the interior of the shaded area, corresponds to a solution of (2.2) that satisfies (2.3). The solid line implies faster (exponential) convergence $f'(\eta) \rightarrow 1$ as $\eta \rightarrow \infty$.

of κ for both front and rear stagnation point flow for which solutions do exist, and to examine the nature of these solutions.

2. Front stagnation point flow

For front stagnation point flow, the outer boundary condition is

$$f'(\eta) \sim +1 \quad \text{as } \eta \rightarrow \infty, \tag{2.1}$$

and (1.7) may be integrated once, using this boundary condition to determine the constant of integration, to give

$$f''' + ff'' - f'^2 + 1 = \kappa \left(\frac{\eta}{2} f'' + f' - 1 \right). \tag{2.2}$$

We have to solve this equation with boundary conditions (from (1.4))

$$f(0) = 0, \quad f'(0) = 0, \quad f'(\infty) = 1, \tag{2.3}$$

We note that (2.2) is also compatible with an unphysical outer boundary condition $f'(\infty) = -(\kappa + 1)$. This problem was first studied by Yang (1958), who computed solutions for a limited range of κ ($-3 < \kappa < +1$), and who inferred by extrapolation that the wall stress (proportional to $f''(0)$) vanishes at $\kappa \approx -3.175$. The question of what happens for $\kappa < -3.175$ was left open, and has (surprisingly) remained open until now.

We have computed solutions by integrating outwards from $\eta = 0$ to a suitably large value of η with three ‘initial’ conditions

$$f(0) = 0, \quad f'(0) = 0, \quad f''(0) = K, \tag{2.4}$$

and then choosing K in such a way as to ensure that $f'(\eta) \sim 1$ for large η (see appendix B for details). Figure 2 shows the values of $K = f''(0)$ thus obtained as a function of κ . Note that the wall stress τ is related to K by $\tau = \rho v^{1/2} K x / [\kappa(t_0 - t)]^{3/2}$, where ρ is the fluid density. For κ positive, K is single-valued, i.e. the velocity profile is unique for accelerating flow. For κ negative (decelerating flow), the situation is

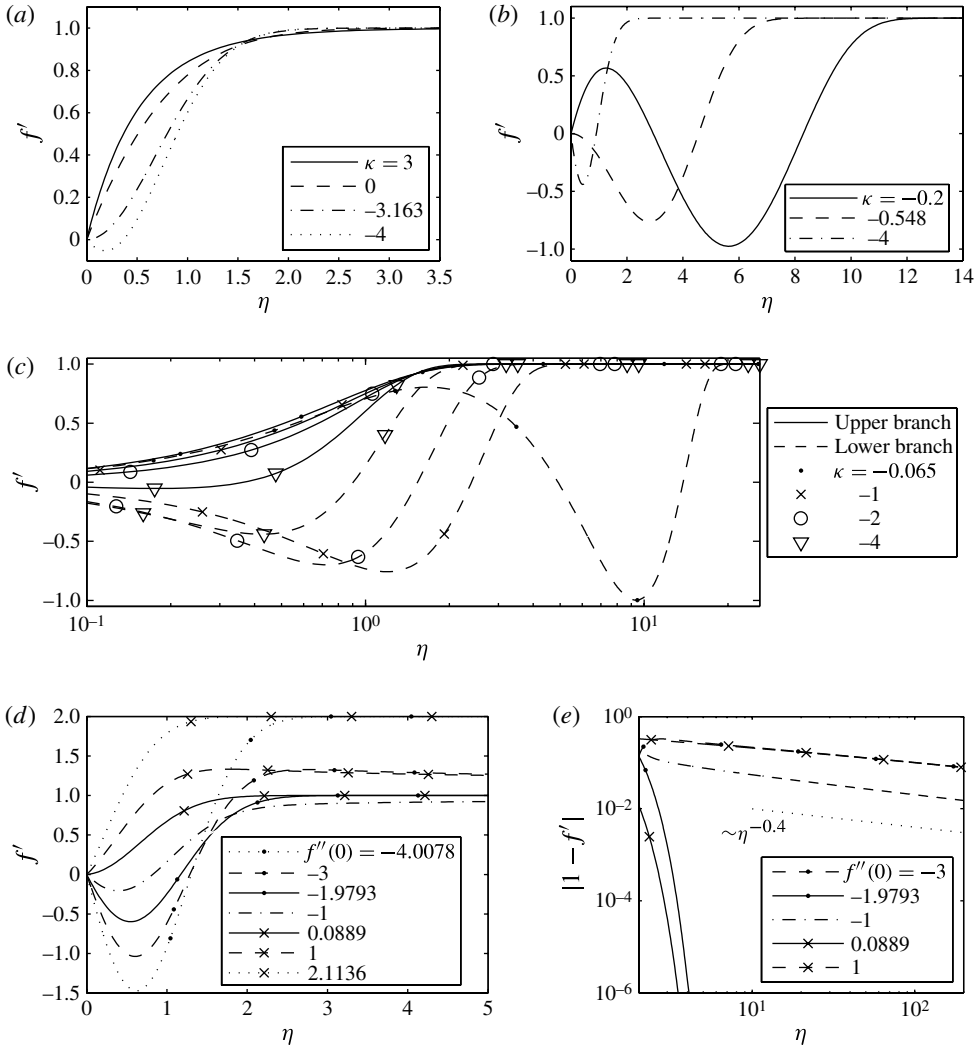


FIGURE 3. Velocity profiles for flows towards a stagnation point. (a) Upper branch and (b) lower branch velocity profiles corresponding to points on the solid curve in figure 2; (c) comparison on a semi-logarithmic scale. (d) Seven different profiles all at $\kappa = -3$; (e) convergence to zero of $|f'(\eta) - 1|$ for five of these solutions, on a logarithmic scale.

more complex, as might be expected. The solution bifurcates into an ‘upper branch’ (partially obtained by Yang 1958) and a ‘lower branch’; these may be followed continuously down to $\kappa \approx -4.6$, where they join. Sample upper and lower branch profiles are shown in figures 3(a) and 3(b), respectively. Four pairs of profiles corresponding to four different values of κ are displayed on a semi-logarithmic scale in figure 3(c). We notice that the upper branch profiles $f'(\eta)$ are positive if $K > 0$, and that the wall stress vanishes at $\kappa \approx -3.163$. The lower branch profiles always have positive and negative parts, regardless of the sign of K . For $\kappa < -2$, there is in addition a one-parameter family of solutions to (2.2)–(2.3) (of which the above upper and lower branch solutions are particular members), as indicated by the shaded area in

figure 2. The range of permissible values of $f''(0)$ is bounded by two solutions of (2.2) with $f'(\infty) = -(\kappa + 1)$, indicated by the dotted boundary curves. For example, for the particular case $\kappa = -3$, any value of $K = f''(0)$ in the open interval $] -4.0078, 2.1136[$ gives a solution for which $f' \rightarrow 1$ as $\eta \rightarrow \infty$. Figure 3(d) shows seven different possible profiles $f'(\eta)$ for this value of κ , including the two ‘limiting’ solutions (for $K = -4.0078$ and 2.1136) and the two that correspond to points on the solid curve within the shaded region in figure 2 ($K = -1.9793$ and $K = 0.0889$). These two are distinguished by exponentially rapid convergence as $\eta \rightarrow \infty$, whereas solutions corresponding to all other values of K in the above open interval converge much more slowly. This will be explained by the large- η asymptotic analysis presented below. The logarithmic plot in figure 3(e) in fact shows that, provided $K \neq -1.9793$ or 0.0889 , $|1 - f'(\eta)| \sim \eta^{-0.4}$ as $\eta \rightarrow \infty$. When K is near to either of the limiting values (-4.0078 or 2.1136), the solution stays near the value $f' = -(\kappa + 1)$ ($=2$ when $\kappa = -3$) to large η before descending to the value $f' = 1$ in the above manner.

Note that each member of this one-parameter family of profiles $f(\eta)$ provides a self-similar solution $\psi(x, y, t)$ that evolves from a corresponding initial condition $\psi(x, y, 0) = \sqrt{\nu A(0)} x f(y/\delta_0)$, with $\delta_0 = (A(0)/\nu)^{-1/2}$.

Large $|\kappa|$ asymptotics

When the unsteadiness parameter $|\kappa|$ is large, (2.2) can be approximated at leading order by

$$g'' = \kappa \left(\frac{\eta}{2} g' + g - 1 \right) \quad \text{where } g = f'. \tag{2.5}$$

In this approximation, the convective (nonlinear) acceleration is negligible compared with the local (linear) acceleration in the Navier–Stokes equation, and (1.3) becomes a linear diffusion equation driven by the time-dependent outer boundary condition. With the change of variable $\theta = |\kappa|^{1/2} \eta/2 = y (|\kappa|A/\nu)^{1/2}/2$ and using an appropriate integrating factor, (2.5) may be reduced to a particular case of Whittaker’s equation (Abramowitz & Stegun 1972, Equation 13.1.31). Here, the sign of κ is crucial. For $\kappa > 0$, the solution satisfying the conditions (2.3) is unique and is given by

$$g = \sqrt{\pi} \theta \operatorname{erfc}(\theta) e^{\theta^2} = 2\theta \int_{\theta}^{\infty} \exp(-(\phi^2 - \theta^2)) d\phi, \quad \kappa > 0. \tag{2.6}$$

(Note that $\int_{\theta}^{\infty} e^{-\phi^2} d\phi \sim (1/2\theta)e^{-\theta^2}$ as $\theta \rightarrow \infty$.) For $\kappa < 0$, however, there is a one-parameter family of solutions satisfying the conditions (2.3):

$$g = (\hat{K} - i\sqrt{\pi} \operatorname{erf}(i\theta)) \theta e^{-\theta^2} = \hat{K}\theta e^{-\theta^2} + 2\theta \int_0^{\theta} \exp(-(\theta^2 - \phi^2)) d\phi, \quad \kappa < 0, \tag{2.7}$$

where the parameter $\hat{K} = g'(0)$ is proportional to the velocity gradient at the boundary $y = 0$. Thus in this case, for each value of $g'(0)$, there is a corresponding similarity solution. We emphasize that this conclusion holds only in the limit $\kappa \rightarrow -\infty$.

Large η asymptotics

We may similarly investigate the existence of solutions for arbitrary κ by examining the asymptotics as $\eta \rightarrow \infty$. Let us assume that a solution of (2.2), (2.3) exists such that $|f'(\eta) - 1|$ is small for $\eta > \eta_m$, where η_m is some suitably large number: $\eta_m \gg 1$.

Then, in this range of large η , we may write

$$f(\eta) = \eta + \int_0^\eta \epsilon(\eta_1) d\eta_1 + E, \quad f'(\eta) = 1 + \epsilon(\eta), \quad f''(\eta) = \epsilon'(\eta), \quad f'''(\eta) = \epsilon''(\eta), \quad (2.8)$$

where E is a constant and ϵ and its derivatives are assumed small. Substitution in (2.2) and linearization gives

$$\epsilon'' + \left(E - \left(\frac{\kappa}{2} - 1 \right) \eta \right) \epsilon' - (2 + \kappa)\epsilon = 0. \quad (2.9)$$

Consider first the particular case $\kappa = 2$, for which the solution to (2.9) is

$$\epsilon(\eta) = C_1 \exp((\sqrt{E^2 + 16} - E)\eta/2) + C_2 \exp(-(\sqrt{E^2 + 16} + E)\eta/2), \quad (2.10)$$

where C_1 and C_2 are constants. Since $\epsilon \rightarrow 0$ as $\eta \rightarrow \infty$, we must have $C_1 = 0$; then C_2 is determined by the condition $\epsilon(\eta_m) = \epsilon_m$, say.

If $\kappa \neq 2$, the general solution of this equation may be expressed in terms of Kummer functions M and U (Abramowitz & Stegun 1972, Equations 13.1.2, 13.1.3):

$$\epsilon(\eta) = C_1 M \left(\frac{\kappa + 2}{\kappa - 2}, \frac{1}{2}; z_1 \right) + C_2 U \left(\frac{\kappa + 2}{\kappa - 2}, \frac{1}{2}; z_1 \right), \quad (2.11)$$

where

$$z_1 = \frac{\kappa - 2}{4} \left(\eta - \frac{2E}{\kappa - 2} \right)^2. \quad (2.12)$$

The asymptotic dependence of U and M on κ and η as $\eta \rightarrow \infty$ is summarized in table 1. There are three distinct regimes of κ .

- (i) For $\kappa > 2$, M diverges exponentially and U decays to zero algebraically. The condition $\epsilon(\infty) = 0$ requires that $C_1 = 0$, then C_2 is determined in terms of $\epsilon(\eta_m)$; if this is assumed known, then the solution is unique.
- (ii) When $-2 < \kappa < 2$, the same condition requires that

$$C_1 = -(-1)^{\kappa-2/\kappa+2} \pi^{-1/2} \Gamma \left(\frac{\kappa + 6}{4 - 2\kappa} \right) C_2, \quad (2.13)$$

and the value of C_2 is again obtained from $\epsilon(\eta_m)$. Note that in the range $-2 < \kappa < 0$, two values of $f''(0)$ lead to convergent solutions of (2.2)–(2.3). These values are nearly equal when κ is small and negative, so the velocity profiles are almost coincident near the boundary, but are very different in an intermediate range of η . Both converge exponentially to 1 as $\eta \rightarrow \infty$. The two profiles are shown in figure 3(c) for the particular value $\kappa = -0.065$. Decreasing $|\kappa|$ shifts the maximum discrepancy to smaller values of η .

- (iii) When $\kappa < -2$, both M and U converge, and we again recognize the existence of a one-parameter family of solutions in this regime. As $\kappa \rightarrow -2 - 0$, the exponent $(4 + 2\kappa)/(2 - \kappa)$ remains negative but tends to zero from below, so the functions M and U decay very slowly with η . However, for $-4.6 < \kappa < -2$, there is a linear combination of M and U that eliminates the leading-order terms and the convergence becomes much faster, in fact exponential; for each κ in this interval this combination yields the two special flows corresponding to the two points on the solid curve in figure 2. Such a pair of velocity profiles for $\kappa = -3$ is shown by the solid lines in figure 3(d,e).

$\kappa < -2$	$-2 < \kappa < 2$	$\kappa > 2$
$M \sim \text{const. } \eta^{(4+2\kappa)/(2-\kappa)} \rightarrow 0$	$M \sim \text{const. } \eta^{(4+2\kappa)/(2-\kappa)} \rightarrow \infty$	$M \sim \text{const. } e^{((\kappa-2)/4)\eta^2} \eta^{(\kappa+6)/(\kappa-2)} \rightarrow \infty$
$U \sim \text{const. } \eta^{(4+2\kappa)/(2-\kappa)} \rightarrow 0$	$U \sim \text{const. } \eta^{(4+2\kappa)/(2-\kappa)} \rightarrow \infty$	$U \sim \text{const. } \eta^{(4+2\kappa)/(2-\kappa)} \rightarrow 0$
$\pi^{-1/2} \Gamma \left(\frac{\kappa+6}{4-2\kappa} \right) M - (-1)^{(\kappa+2)/(\kappa-2)} U \sim$ $\text{const. } e^{((\kappa-2)/4)\eta^2} \eta^{(\kappa+6)/(\kappa-2)} \rightarrow 0$		

TABLE 1. Asymptotics of (2.11) as $\eta \rightarrow \infty$.

$\kappa < -2$	$-2 < \kappa < 2$	$\kappa > 2$
$M \sim \text{const. } \eta^{(4-2\kappa)/(2+\kappa)} \rightarrow 0$	$M \sim \text{const. } e^{((\kappa+2)/4)\eta^2} \eta^{(\kappa-6)/(\kappa+2)} \rightarrow \infty$	$M \sim \text{const. } e^{((\kappa+2)/4)\eta^2} \eta^{(\kappa-6)/(\kappa+2)} \rightarrow \infty$
$U \sim \text{const. } \eta^{(4-2\kappa)/(2+\kappa)} \rightarrow 0$	$U \sim \text{const. } \eta^{(4-2\kappa)/(2+\kappa)} \rightarrow \infty$	$U \sim \text{const. } \eta^{(4-2\kappa)/(2+\kappa)} \rightarrow 0$

TABLE 2. Asymptotics to (3.8) as $\eta \rightarrow \infty$.

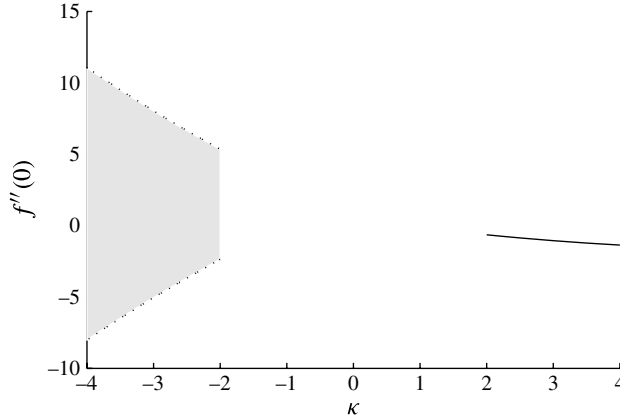


FIGURE 4. Velocity gradient at the wall in flows away from a stagnation point. A solution to (3.1)–(3.2) exists if $(\kappa, f''(0))$ lies either on the solid line or in the shaded area. The dashed lines that bound the shaded area correspond to solutions of (3.1) with $f'(\infty) = 1 - \kappa$.

In the limit $\kappa \rightarrow \infty$, M diverges and the only convergent solution is $U \sim \eta^{-2}$, in agreement with the asymptotic expansion of (2.6),

$$g(\theta) \sim 1 - \frac{1}{2\theta^2} + O(\theta^{-4}) \quad \text{as } \theta \rightarrow \infty. \tag{2.14}$$

When $\kappa \rightarrow -\infty$, both M and U decay like η^{-2} . The corresponding asymptotic approximation to (2.7) is

$$g(\theta) \sim 1 + \frac{1}{2\theta^2} + O(\theta^{-4}) \quad \text{as } \theta \rightarrow \infty. \tag{2.15}$$

Its leading terms do not involve the arbitrary constant \hat{K} as they derive from the term $i\sqrt{\pi} \operatorname{erf}(i\theta) \theta e^{-\theta^2}$, so all solutions converge equally fast when κ is large and negative.

3. Rear stagnation point flow

When $U(x, t) = -A(t)x$, the streamfunction can again be sought in the form (1.5), where $f(\eta)$ must now satisfy

$$f''' + ff'' - f'^2 + 1 = \kappa \left(\frac{\eta}{2} f'' + f' + 1 \right), \tag{3.1}$$

$$f(0) = 0, \quad f'(0) = 0, \quad f'(\infty) = -1, \tag{3.2}$$

with κ still defined by (1.8).

If $\kappa = 0$, then as already noted, this problem has no solution. However, solutions do exist when $|\kappa|$ is large enough. Figure 4 shows the values of $f''(0)$ consistent with the outer boundary condition $f'(\infty) = -1$. Now there are two distinct regimes.

- (i) For any $\kappa \geq 2$, there is a unique profile $f'(\eta)$. Figure 5(a) shows some of these. The convergence is very slow compared with that for accelerating flow towards a stagnation point (cf. figure 3a). In the limiting case $\kappa = 2$, f' approaches -1 like

$$f' \sim \frac{2}{\ln C\eta} - 1 \quad \text{as } \eta \rightarrow \infty, \tag{3.3}$$

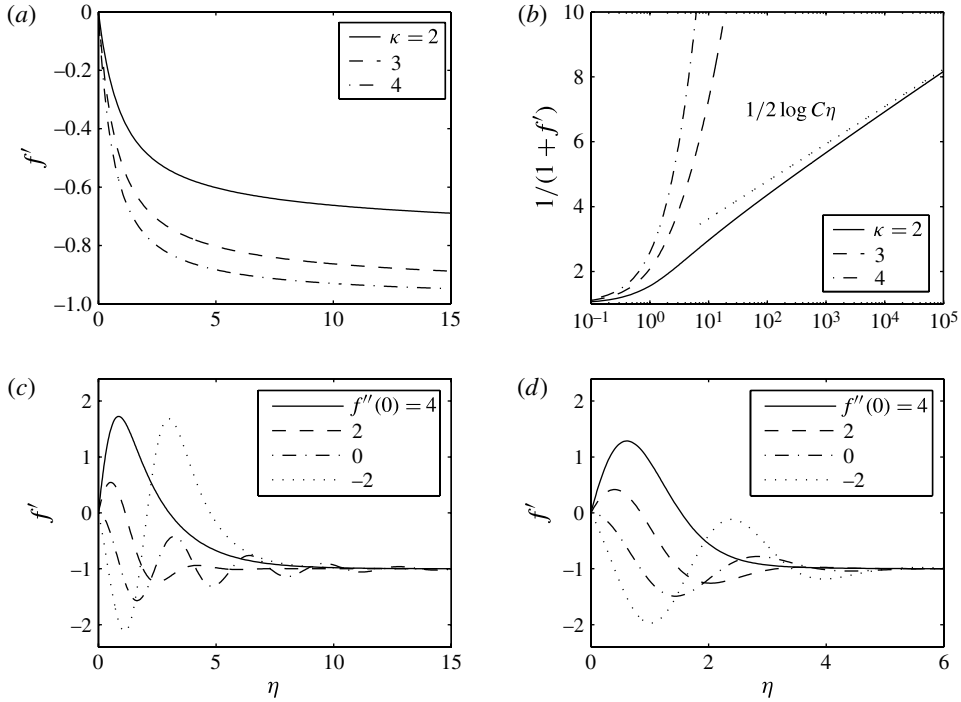


FIGURE 5. (a) Velocity profiles $f'(\eta)$ and (b) an inverse of the residual $1/(1+f'(\eta))$ for accelerating flows away from a stagnation point. Velocity profiles for decelerating flows away from a stagnation point at (c) $\kappa = -2$ and (d) $\kappa = -3$.

where $C \approx 140$. Figure 5(b) shows the inverse of the residual $1/(1+f'(\eta))$, in a semi-logarithmic plot, for a wide range of η . This confirms (3.3) and indicates that the convergence is much faster when $\kappa - 2$ is not small.

(ii) For any $\kappa \leq -2$ there is a one-parameter family of solutions. Such pairs $(\kappa, f''(0))$ lie in the shaded area in figure 4. Some sample velocity profiles $f'(\eta)$ for $\kappa = -2$ and $\kappa = -3$ are shown in figure 5(c,d).

In the large $|\kappa|$ approximation, the solution to (3.1)–(3.2) has the asymptotic behaviour

$$f' \sim -\sqrt{\pi} \theta \operatorname{erfc}(\theta) e^{\theta^2}, \quad \kappa > 0, \tag{3.4}$$

$$f' \sim (\hat{K} + i\sqrt{\pi} \operatorname{erf}(i\theta)) \theta e^{-\theta^2}, \quad \kappa < 0. \tag{3.5}$$

Note that these differ from (2.6) and (2.7) only in sign, as is to be expected in this linearized situation.

The complementary linearization for large η is

$$f(\eta) = -\eta + \int_0^\eta \epsilon(\eta_1) d\eta_1 + E, \quad f'(\eta) = -1 + \epsilon(\eta), \quad f''(\eta) = \epsilon'(\eta), \quad f'''(\eta) = \epsilon''(\eta), \tag{3.6}$$

$$\epsilon'' + \left(E - \left(\frac{\kappa}{2} + 1 \right) \eta \right) \epsilon' + (2 - \kappa)\epsilon = 0, \tag{3.7}$$

where E is a constant. Excluding exceptional values which will be discussed below ($\kappa \neq -2$; $(6 - \kappa/4 + 2\kappa) \neq -1, -2, \dots$ when $\kappa < -2$; $(\kappa - 2/\kappa + 2) \neq -1, -2, \dots$

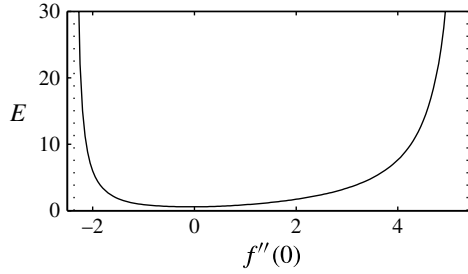


FIGURE 6. A numerical estimate of E as a function of $f''(0)$ for $\kappa = -2$; see (3.10). Dots mark the limits $f''(0) \approx -2.369$ and 5.363 .

when $-2 < \kappa < 2$), the solution is

$$\epsilon(\eta) = C_1 M \left(\frac{\kappa - 2}{\kappa + 2}, \frac{1}{2}; z_2 \right) + C_2 U \left(\frac{\kappa - 2}{\kappa + 2}, \frac{1}{2}; z_2 \right), \tag{3.8}$$

where now

$$z_2 = \frac{\kappa + 2}{4} \left(\eta - \frac{2E}{\kappa + 2} \right)^2. \tag{3.9}$$

The asymptotics for $\eta \rightarrow \infty$ are shown in table 2. The key difference from the case of flow towards a stagnation point is in the range $-2 < \kappa < 2$. Here, M now diverges exponentially while U still diverges as a power of η , so no non-trivial choice of C_1, C_2 can yield a decaying solution. There exist exceptional values $\kappa = 2(1 - n)/(1 + n)$, $n \in \mathbb{N}$ (see appendix A) for which M and U are exactly proportional and the complete solution is different from (3.8), but again it is a linear combination of two terms that diverge like $\eta^{(\kappa-6)/(\kappa+2)} \exp((\kappa + 2)\eta^2/4)$ and $\eta^{(4-2\kappa)/(2+\kappa)}$. In every case, the linearized problem has no convergent solution when $|\kappa| < 2$, in agreement with the numerical results for the original nonlinear problem.

When $\kappa > 2$, U converges like $\eta^{-\zeta}$ with $\zeta = 2(\kappa - 2)/(2 + \kappa)$ (in the range $0 < \zeta < 2$). This is again consistent with the slow convergence observed in the numerical solution in figure 5(a). When $\kappa < -2$, $\zeta > 2$ and both M and U decay faster. Exceptional cases $(6 - \kappa)/(4 + 2\kappa) = -1, -2, \dots$ can arise, but the rate of decay remains unchanged. In the particular case $\kappa = -2$ the solution to (3.7) is

$$\epsilon(\eta) = C_1 \exp((\sqrt{E^2 - 16} - E)\eta/2) + C_2 \exp(-(\sqrt{E^2 - 16} + E)\eta/2), \tag{3.10}$$

which decays if $E > 0$ for any values of the constants C_1 and C_2 . The value of E of course depends on the behaviour of $f(\eta)$ in the region of its rapid variation near $\eta = 0$ where the nonlinearity is important. Figure 6 shows E versus $f''(0)$, estimated by matching (3.10) to the numerical solution of the nonlinear problem (3.1)–(3.2) at $\eta_m = 18$. Substituting (3.10) into the three last equations of (3.6) gives a closed system for E, C_1 and C_2 , from which it follows that

$$E = -\frac{f'''(\eta_m) + 4 + 4f'(\eta_m)}{f''(\eta_m)}. \tag{3.11}$$

E is strictly positive in the interval $f''(0) \in [-2.369, 5.363]$. However, the rate of decay of $\epsilon(\eta)$ is very slow near the ends of the interval, where $E \rightarrow \infty$ and $\sqrt{E^2 - 16} - E \sim -8/E$.

4. Discussion and conclusions

Unsteady stagnation point flows may admit self-similar solutions (1.5) when the flow strength varies in time according to (1.9), in which the dimensionless parameter κ provides a measure of the unsteadiness of the flow. Our main conclusions may be summarized as follows.

- (i) In an accelerating front stagnation point flow, there is a unique velocity profile $f'(\eta)$ for any $\kappa > 0$. This flow may be regarded as a straightforward modification of the steady flow of Hiemenz (1911).
- (ii) In a decelerating front stagnation point flow, there are two possible profiles when $-2 < \kappa < 0$ and a one-parameter family of profiles when $\kappa \leq -2$. The two special profiles may be followed down to $\kappa \approx -4.6$, and are characterized by exponential convergence for large η , in contrast to all other solutions in the one-parameter family, which converge algebraically.
- (iii) In an accelerating rear stagnation point flow, a solution exists only when $\kappa \geq 2$ and it is unique. The existence of this flow may appear counter-intuitive; however, it is best understood by consideration of the large κ limit, in which the governing equation becomes linear, so that if $\psi(x, y, t)$ is a solution then so is $-\psi(x, y, t)$. Thus the solution in this limit is effectively the same (but with reversed arrows on the streamlines) as that for the front stagnation flow case. As κ is reduced, this solution is increasingly modified by convective (nonlinear) acceleration, until, at $\kappa = 2$, the solution ceases to exist.
- (iv) In a decelerating rear stagnation point flow, there is no solution for $-2 < \kappa \leq 0$, but there exists a one-parameter family of profiles for any $\kappa \leq -2$. Here, the existence of solutions for $\kappa < -2$ may be understood by the following argument. Outside the boundary layer, the time-dependent strain field convects fluid in the positive y -direction at speed $dy/dt = (-\kappa)^{-1} y (t - t_0)^{-1}$, with solution $y \sim (t - t_0)^{(-1/\kappa)}$. This may be compared with the natural viscous growth of a boundary layer $\delta \sim (t - t_0)^{1/2}$. Thus, if $\kappa < -2$, the viscous growth is more rapid than the convective transport away from the boundary, and a growing boundary layer, controlled by viscosity, is possible. If, on the other hand, $-2 < \kappa < 0$, then convection wins (as for the impulsive situation considered e.g. by Proudman & Johnson 1962), and no boundary-layer solution is possible.
- (v) When $|\kappa|$ is large, then, as indicated above, the convective acceleration is negligible compared with the local acceleration, and the corresponding velocity profiles can be obtained in analytic form, as given in (2.6), (2.7), (3.4) and (3.5).

These self-similar solutions may be used to extend our previous analysis of the clap-fling-sweep mechanism (Kolomenskiy *et al.* 2011) to the large-Reynolds-number situation. Further, the flow could be realized in an experiment and the resulting flow field compared with the theoretical results. In particular, it would be interesting to see the range of initial conditions for which the similarity solutions are realized and what happens in the ranges where no solutions are predicted.

Finally, we may note that a very similar situation is to be expected for three-dimensional stagnation point flows. Williams (1968), Cheng, Özişik & Williams (1971) and Teipel (1979) have obtained self-similar solutions for flows towards the stagnation point. This needs to be extended to the corresponding rear stagnation point flows.

Acknowledgements

D.K. gratefully acknowledges support from the David Crighton Fellowship and thanks DAMTP, University of Cambridge, for the hospitality.

Appendix A. Asymptotic expansion of Kummer functions M and U

The asymptotic expansion of $M(a, b; z)$ and $U(a, b; z)$ for $z \in \mathbb{C}$, $|z|$ large and $a, b \in \mathbb{R}$ fixed, is (Abramowitz & Stegun 1972, Equations 13.5.1 and 13.5.2)

$$\frac{M(a, b; z)}{\Gamma(b)} = \frac{e^{\pm i\pi a} z^{-a}}{\Gamma(b-a)} \left\{ \sum_{n=0}^{R-1} \frac{(a)_n (1+a-b)_n}{n!} (-z)^{-n} + O(|z|^{-R}) \right\} + \frac{e^z z^{a-b}}{\Gamma(a)} \left\{ \sum_{n=0}^{S-1} \frac{(b-a)_n (1-a)_n}{n!} z^{-n} + O(|z|^{-S}) \right\}, \tag{A 1}$$

where the upper sign is taken if $-\frac{1}{2}\pi < \arg z < \frac{3}{2}\pi$, the lower sign if $-\frac{3}{2}\pi < \arg z \leq -\frac{1}{2}\pi$ and $(a)_n = a(a+1)(a+2) \cdots (a+n-1)$, $(a)_0 = 1$. Further

$$U(a, b; z) = z^{-a} \left\{ \sum_{n=0}^{R-1} \frac{(a)_n (1+a-b)_n}{n!} (-z)^{-n} + O(|z|^{-R}) \right\}, \tag{A 2}$$

where $-\frac{3}{2}\pi < \arg z < \frac{3}{2}\pi$. In (2.11) and (3.8), z is real. Depending on its sign, either the first or the second curly bracket in (A 1) dominates, leading to the exponential and algebraical regimes listed in tables 1 and 2. If $a = -1, -2, \dots$ or $b - a = -1, -2, \dots$, either $\Gamma(a)$ or $\Gamma(b - a)$ diverges and the corresponding curly bracket vanishes, hence the exceptional cases.

Appendix B. Numerical solution of (2.2) and (3.1)

Three different methods of numerical solution of (2.2) and (3.1) have been used.

B.1. Newton’s method

This is a standard method for solving nonlinear boundary-value problems on a closed interval. The iterative solver is applied to an equivalent system of nonlinear first-order differential equations,

$$\begin{aligned} f' &= f_1, \\ f_1' &= f_2, \\ f_2' &= -ff_2 + f_1^2 - 1 + \kappa \left(\frac{\eta}{2} f_2 + f_1 \mp 1 \right), \end{aligned} \tag{B 1}$$

with boundary conditions imposed at the ends of a sufficiently large interval,

$$f(0) = f_1(0) = 0, \quad f_1(\eta_{max}) = \pm 1. \tag{B 2}$$

The upper/lower sign is taken for front/rear stagnation point flow, respectively. A sequence of values of η_{max} is taken in order to obtain the desired accuracy. The system (B 1)–(B 2) was solved using the BVP4C function in MATLAB (Kierzenka & Shampine 2001), which is a finite-difference code that implements the three-stage Lobatto IIIa formula, which is fourth-order accurate. In our case, it can only be used if $|f'(\eta) - f'(\infty)|$ decays rapidly enough. When η_{max} is very large, the Jacobian matrix becomes ill-conditioned and the method fails. Moreover, this method gives only one solution.

B.2. Shooting method

An alternative method, that can be used when the solution is not unique, is to assume a value of $f_2(0)$ and solve (B 1)–(B 2) as an initial-value problem using a Runge–Kutta method. We used the ODE45 function in MATLAB, which is based on a Dormand–Prince pair (Dormand & Prince 1980) and adapts the discretization step to ensure the desired accuracy. It was set to 10^{-11} in most of our computations. The convergence of the numerical solution to the initial-value problem for a given value of $f''(0)$ is guaranteed (see e.g. §7.2 in the book by Stoer & Bulirsch 1983). One has to check *a posteriori* whether $f'(\eta)$ tends to 1 or -1 as η goes to η_{max} . To find the value of $f''(0)$ consistent with the condition at $\eta \rightarrow \eta_{max}$, the bisection method was used. It converges to a solution if the initial interval is chosen such that the function changes sign. A search throughout the κ – $f''(0)$ plane is made beforehand to locate such intervals. The value of $f''(0)$ was typically calculated with an accuracy of 10^{-6} – 10^{-8} .

B.3. Iterative method based on the linearization

Neither of these methods can be used for the case of accelerating flow away from a stagnation point. A very large value of η_{max} is needed, because the velocity profile converges very slowly. It was shown in §3 that one of the two terms in the complete solution of the linearized equation (3.7) diverges exponentially. Therefore, for a Runge–Kutta integration, an extremely precise estimate of $f''(0)$ is required for matching the condition at η_{max} . In this situation, it was found more efficient to use the iterative method described below.

From (3.1)–(3.2), the change of variables $\theta = |\kappa|^{1/2} \eta/2$, $h(\theta) = |\kappa|^{1/2} f(\eta)/2$, leads to

$$h''' + p \left(hh'' - h'^2 + 1 \right) = q \left(\frac{\theta}{2} h'' + h' + 1 \right), \tag{B 3}$$

where $p = 4/|\kappa|$, $q = 4\kappa/|\kappa|$ and primes denote derivatives with respect to θ . Let h_0 be an approximation to h and $\epsilon = h' - h'_0$. If ϵ is small, linearization gives

$$\begin{aligned} -\epsilon'' + \epsilon' \left(\frac{q\theta}{2} - ph_0 \right) + \epsilon [q + p(h'_0 - 1)] \\ = h_0''' - h_0'' \left(\frac{q\theta}{2} - ph_0 \right) - [q + p(h'_0 - 1)] (h'_0 + 1), \end{aligned} \tag{B 4}$$

with boundary conditions $\epsilon(0) = 0$, $\epsilon(\theta_{max}) = 0$. Equation (B 4) is discretized using a second-order finite-difference scheme. The system of linear algebraic equations gives ϵ , and then numerical integration gives a new approximation to h ,

$$h_1 = h_0 + \int_0^{\theta_{max}} \epsilon \, d\theta, \tag{B 5}$$

which replaces h_0 in (B 4) and the equation is then solved again. The process is repeated until the desired accuracy is reached.

In order to check the correctness of this numerical solution, the following tests were carried out. The numerical solution $f'_{(N)}$ was calculated on grids with $N = N_{min} \dots N_{max}$ points, where $N_{min} = 2^7$, $N_{max} = 2^{24}$. For each N , the number of iterations (every iteration involves a solution of the linearized equation (B 4)) was chosen to be equal to $\log_2(N/N_{min}) + 1$. The far-field boundary condition $\epsilon(\theta_{max}) = 0$ was imposed

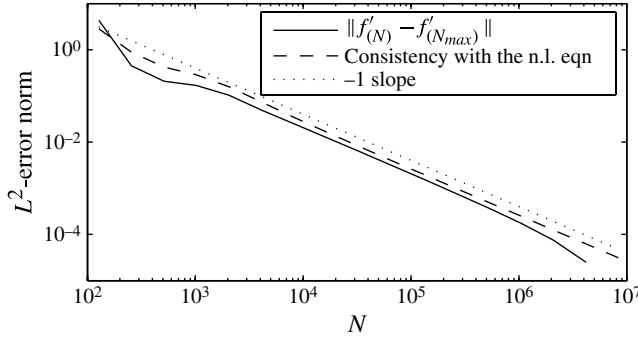


FIGURE 7. Convergence of the numerical solution for the rear stagnation point flow with $\kappa = 3$.

at $\theta_{max} = 1000$, and the $L^2([0, \theta_{max}/2])$ -norm of the difference between $f'_{(N)}$ and $f'_{(N_{max})}$ was calculated. This is shown with a solid line in figure 7. It provides evidence that the numerical solution converges. In addition, the $f_{(N)}$ thus obtained were tested *a posteriori* for their consistency with a finite-difference approximation of the nonlinear equation (3.1). Second-order central finite differences were used to calculate $f''_{(N)}$ and $f'''_{(N)}$. The trapezoidal integration rule was used for $f_{(N)}$. The L^2 -norm of the residual $f'''_{(N)} + f_{(N)}f''_{(N)} - f'^2_{(N)} + 1 - \kappa(\eta f''_{(N)}/2 + f'_{(N)} + 1)$ is shown in figure 7 with a dashed line. It also converges, indicating that $f_{(N)}$ tends to the exact solution of the original differential equation as $N \rightarrow \infty$.

Appendix C. Numerical examples of unsteady flows past an array of circular cylinders.

Numerical simulations were performed in order to check if the self-similar boundary-layer profiles are realized near the stagnation points at the surface of a bluff body accelerating or decelerating in a fluid. The flow past an array of cylinders was modelled. The Navier–Stokes equations were solved using a Fourier pseudo-spectral method, assuming that the computational domain is rectangular and periodic conditions are imposed at its boundary. In the present computations, the periodic domain size is $L_x \times L_y = 3 \times 3$. A circular cylinder of radius $R = 1$ is placed in its centre. The cylinder starts impulsively at $t = 0$, then moves so that its velocity equals

$$U_c = \frac{RA(t)}{2c_{per}} \quad \text{where } A(t) = \frac{1}{\kappa(t_0 - t)}. \quad (\text{C } 1)$$

Two computations were carried out: an accelerating flow ($\kappa = 3$, $t_0 = 2$) and a decelerating flow ($\kappa = -3$, $t_0 = -0.2$). The constant c_{per} equals 1 for an isolated cylinder, which would be equivalent to the periodic boundary conditions being imposed at infinity. A potential flow calculation gave the value $c_{per} \approx 0.99$ for $L_x \times L_y = 3 \times 3$. The viscosity equals $\nu = 10^{-4}$. The grid size is $N_x \times N_y = 12\,000 \times 12\,000$ points, which is enough to well resolve the boundary layer up to $t = 1.8$ in the accelerating case. The solid boundary was modelled using the volume penalization method with penalization parameter $\eta = 3 \times 10^{-4}$. More details about this method and its implementation can be found in the papers by Angot, Bruneau & Fabrie (1999), Schneider (2005) and Kolomenskiy & Schneider (2009).

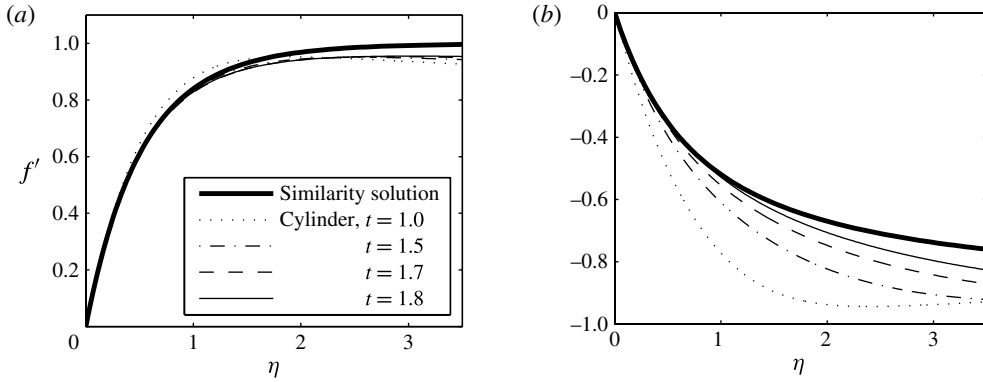


FIGURE 8. Boundary-layer profiles near the (a) front and (b) rear stagnation points of an accelerating cylinder, reduced to the similarity variables. Time instants $t = 1.0, 1.5, 1.7$ and 1.8 . Azimuthal position $\theta = 5^\circ$, measured from the corresponding stagnation point.

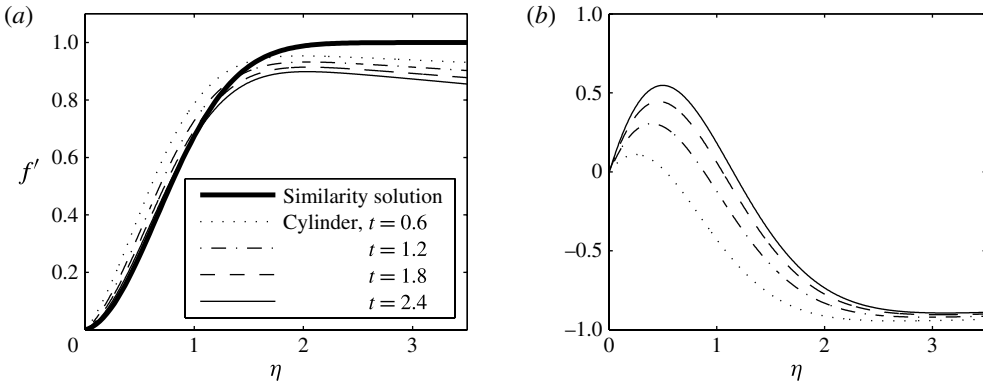


FIGURE 9. Boundary-layer profiles near the (a) front and (b) rear stagnation points of a decelerating cylinder, reduced to the similarity variables. Time instants $t = 0.6, 1.2, 1.8$ and 2.4 . Azimuthal position $\theta = 5^\circ$, measured from the corresponding stagnation point. The thick line in figure (a) shows the similarity solution for $f''(0) = 0.0889$.

The velocity profiles of the accelerating flow are compared in figure 8. After the flow starts impulsively, the initial evolution of the boundary layer is mainly driven by the viscous stresses. The front and rear profiles are almost symmetric. Then the flow evolves to its self-similar state. The profiles obtained numerically converge with time to their unique self-similar shapes on both sides of the cylinder. The front profile converges faster than the rear one. In both cases, there is a visible discrepancy at $\eta > 1$: in the numerical simulation, the profiles do not tend to their large-Reynolds-number limit of ± 1 . Obviously, the accuracy of the boundary-layer theory is not fully satisfactory at $Re \approx 10^4$, but well-resolved numerical simulations at larger values of Re are not feasible for the present method.

In the decelerating flow, the velocity profiles have inflection points, as shown in figure 9. Moreover, there is a flow reversal near the rear stagnation point. At both sides of the cylinder, the similarity solutions are not unique. The front profiles converge to the self-similar shape corresponding to $f''(0) = 0.0889$, which results in the thinnest

possible boundary layer. The rear profiles may be converging to the self-similar shape with $f''(0) = 4$, but as the Reynolds number of this flow decreases in time, the discrepancy increases in the outer part of the boundary layer.

These numerical simulations provide evidence that the similarity solutions are attracting for the accelerating flow past a cylinder at both stagnation points, and for the decelerating flow at the front stagnation point. An exhaustive numerical study of all possible regimes would require many more simulations and a proper method. The value of the similarity solutions is to provide some basic insight before carrying out such long computations.

REFERENCES

- ABRAMOWITZ, M. & STEGUN, I. 1972 *Handbook of Mathematical Functions with Formulas, Graphs, and Mathematical Tables*, 10th edition. Dover.
- ANGOT, P., BRUNEAU, C.-H. & FABRIE, P. 1999 A penalization method to take into account obstacles in viscous flows. *Numer. Math.* **81**, 497–520.
- BURDE, G. I. 1995 The construction of special explicit solutions of the boundary-layer equations: unsteady flows. *Q. J. Mech. Appl. Math.* **48** (4), 611–633.
- CHENG, E. H. W., ÖZİŞİK, M. N. & WILLIAMS, J. C. III 1971 Nonsteady three-dimensional stagnation-point flow. *J. Appl. Mech.* **38** (1), 282–287.
- DORMAND, J. R. & PRINCE, P. J. 1980 A family of embedded Runge–Kutta formulae. *J. Comput. Appl. Math.* **6**, 19–26.
- DRAZIN, P. & RILEY, N. 2006 *The Navier–Stokes Equations: A Classification of Flows and Exact Solutions*. Cambridge.
- EDWARDS, R. H. & CHENG, H. K. 1982 The separation vortex in the Weis-Fogh circulation-generation mechanism. *J. Fluid Mech.* **120**, 463–473.
- HIEMENZ, K. 1911 Die Grenzschicht an einem in den gleichförmigen Flüssigkeitsstrom eingetauchten geraden Kreiszyylinder. *Dingl. Polytech. J.* **326**, 321–410.
- KIERZENKA, J. & SHAMPINE, L. F. 2001 A BVP solver based on residual control and the MATLAB PSE. *ACM Trans. Math. Softw.* **27** (3), 299–316.
- KOLOMENSKIY, D., MOFFATT, H. K., FARGE, M. & SCHNEIDER, K. 2011 The Lighthill–Weis-Fogh clap–fling–sweep mechanism revisited. *J. Fluid Mech.* **676**, 572–606.
- KOLOMENSKIY, D. & SCHNEIDER, K. 2009 A Fourier spectral method for the Navier–Stokes equations with volume penalization for moving solid obstacles. *J. Comput. Phys.* **228**, 5687–5709.
- LIGHTHILL, M. J. 1973 On the Weis-Fogh mechanism of lift generation. *J. Fluid Mech.* **60** (1), 1–17.
- PROUDMAN, I. & JOHNSON, K. 1962 Boundary-layer growth near a rear stagnation point. *J. Fluid Mech.* **12** (2), 161–168.
- SCHLICHTING, H. 1960 *Boundary Layer Theory*, 4th edition. McGraw-Hill.
- SCHNEIDER, K. 2005 Numerical simulation of the transient flow behaviour in chemical reactors using a penalization method. *Comput. Fluids* **34**, 1223–1238.
- STOER, J. & BULIRSCH, R. 1983 *Introduction to Numerical Analysis*. Springer.
- TEIPEL, I. 1979 Unsteady laminar boundary layers in an incompressible three-dimensional stagnation flow. In *Recent Developments in Theoretical and Experimental Fluid Mechanics: Compressible and Incompressible Flows* (ed. U. Müller, K. G. Roesner & B. Schmidt), pp. 439–445. Springer.
- WILLIAMS, J. C. III 1968 Nonsteady stagnation-point flow. *AIAA J.* **6** (12), 2417–2419.
- YANG, K.-T. 1958 On unsteady laminar boundary layers. *Trans. ASME: J. Appl. Mech.* **25**, 421–427.